



Cansmart 2005

International Workshop

SMART MATERIALS AND STRUCTURES

13 - 14 October 2005, Toronto, Ontario, Canada

**DYNAMIC MODELLING OF A COMPLEMENTARY CLAMP
PIEZOWORM™ ACTUATOR**

S. Salisbury¹, D. Waechter², R. Ben Mrad¹, R. Blacow², B. Yan², and S. E. Prasad²

¹Department of Mechanical and Industrial Engineering, University of Toronto

²Sensor Technology Limited, Collingwood, ON

ABSTRACT

A piezoworm step-and-repeat type actuator is being developed which uses complementary configurations for the two clamping sections. The clamps engage on opposite extremes of the common clamp signal—while one clamp engages with high voltage, the other releases at high voltage and vice versa for low voltage. This allows the actuator to be driven with a two-channel controller instead of the usual three-channel controller. A diode-shunted delay circuit that causes unclamping to occur more slowly than clamping can be added in series with each clamp. This increases the overall force drive capability of the actuator. The performance is also influenced by the timing of the common clamp signal relative to the extender signal as well as the signal waveform shapes. In this paper, the dynamic model of the actuator is presented which includes the electrical, mechanical and friction behaviour of the piezomotor components. This model is then used to assess different voltage waveforms input to the actuator and delay circuit resistances in order to optimize the performance.

Keywords: actuator, complementary, piezoelectric.

1. INTRODUCTION

One way piezoelectric actuators achieve long range motion is to be configured in a step-and-repeat type arrangement which uses a repeating clamp-extend-clamp cycle [1]. They typically use two piezoelectric actuators for two clamp sections and a third for the extender section [2]. The specific form and timing of the waveforms for each actuator can influence the piezoworm performance [3-5].

While hybrid piezoworm actuators have been proposed in which the clamp and extender sections use different actuation technologies [6, 7], it is most often the case that the two clamp sections use the same actuation technology in an identical configuration. In the piezoworm design, we utilize complementary clamps in which one clamp grips with low voltage and releases with high voltage while the other grips with high voltage and is released with low voltage. These are referred to as normally clamped (NC) and normally unclamped (NU) respectively. Complementary clamps make it possible to drive the piezoworm actuator with a 2-channel controller with the two clamps sharing a common channel [8] which reduces the drive electronics required. It is also possible to enter the fine positioning mode with both clamps unpowered. A diode-shunted resistive delay circuit can be added in series into each clamp signal which slows the rate of unclamping relative to clamping. The circuit is used in order to increase the total restraining force of the two clamps during the switching transient, thereby increasing the overall force drive capability of the actuator [8].

This paper presents a complementary piezoworm design, a dynamic model with friction characterization and waveform assessment through simulation. Section 2 describes the general concept of complementary piezoworm actuator with some clamp designs and also describes the delay circuit. Section 3 describes the dynamic model and Section 4 then presents the simulation results for different waveforms. Conclusions are summarized in Section 5.

2. ACTUATOR CONCEPT

A general configuration of a linear complementary piezoworm actuator is shown in Fig. 1. The actuator has one NC and one NU type clamp. Either may be stationary but when high speed is required, the clamp type with the smaller mass is normally used as the mobile clamp. The extender actuator separates the two clamps and a spring mechanism returns it to the original position when the extender is de-energized. In the configuration shown, the body of the actuator is fixed and a plate termed the moving member performs the motion.

In the case where the NC clamp is mobile and the NU clamp is stationary, a fine positioning mode can be realized with both clamps unpowered. In this mode, extender activation finely adjusts the moving member position within a range determined by the maximum extender expansion. In the case where the NU clamp is mobile and the NC clamp is stationary, the fine positioning mode requires high voltage on the two clamps. But also in this case, the unpowered actuator presents a larger horizontal stiffness to the moving member and will be free from any creep effects associated with the extender stack or compression spring. [8]

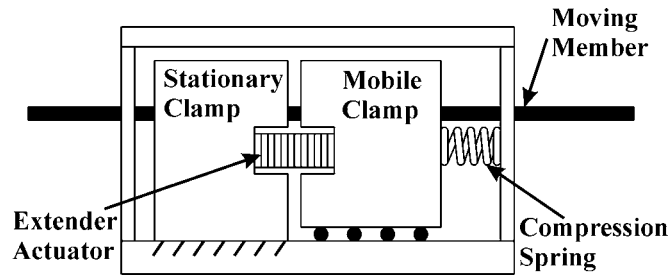


Fig. 1: General complementary piezoworm actuator configuration.

Design configurations for the NU and NC clamps are illustrated in Fig. 2 along with the corresponding restraining force vs. applied voltage characteristics assuming a constant coefficient of friction. For the NU clamp of Fig. 2a), a multilayer piezoelectric stack is supported in a flexure frame in order to maintain a moderate pre-stress and protect the stack from shear forces imparted by the moving member. An upper clamping surface is suspended above the moving member and held in place by front and back face-plates (not shown in the figure). The position of the unobstructed upper clamping surface can be adjusted by set-screw rotation. The NU clamp is adjusted so that with zero voltage on the piezoelectric stack, the gap between the two clamping surfaces slightly exceeds the moving member thickness resulting in zero clamping force. The clamping threshold voltage, V_{TNU} , is the piezoelectric stack voltage at which the separation of the two clamping surfaces first equals the moving member thickness. Beyond V_{TNU} , the restraining force on the moving member begins to rise. The subsequent slope of the restraining force vs. voltage characteristic depends on the properties of the piezoelectric stack, the stiffness of the upper clamping flexure and the coefficient of friction between the moving member and clamping surfaces. The force, F_{MAX} , denotes the maximum restraining force corresponding to the maximum permissible applied voltage for the stack actuator.

Fig. 2b) shows a possible configuration for the NC clamp. It is essentially the same as the NU clamp of Fig. 2a) except that the piezoelectric stack is oriented horizontally and acts through a Cymbal-style flexure [9]. Cymbal flexures can incorporate amplification at the cost of stiffness [10]. This clamp configuration would be designed to have an amplification of unity in order to have the same F_{MAX} and $|dF/dV|$ of the NU clamp in Fig. 2a). The clamping threshold voltage, V_{TNC} , is the piezoelectric stack voltage at which the clamping surface first separates from the moving member. The designs of Figs. 2a) and 2b) have close to the same mass and either could be used as the mobile clamp. The choice will ultimately depend on whether it is preferred to have the moving member fixed to the stationary clamp or subject to fine positioning control when the clamp voltages are zero. Other clamp designs are detailed in [8].

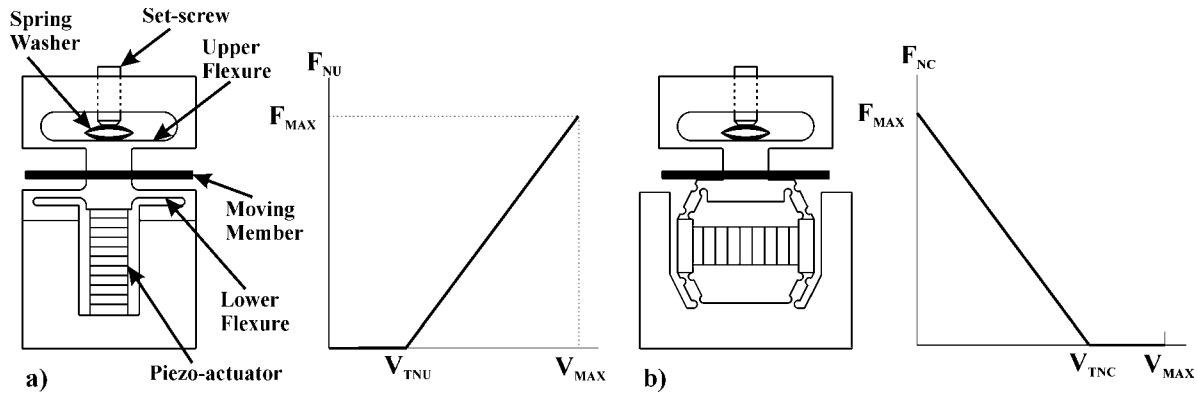


Fig. 2: Clamp configurations with their restraining force-voltage characteristics, a) NU clamp, b) Cymbal-style NC clamp.

Fig. 3 shows the resistive delay circuit connected to each clamp with a common clamp input voltage, V_C . The circuit assumes subresonant operation where the piezostack actuators can be modelled as simple capacitors having values C_{NU} and C_{NC} . A diode-shunted resistance, R , is placed in series with each clamp. The diodes are oriented in different directions so that for each clamp type, the resistance is bypassed during the clamping operation and the clamp voltage closely follows the input signal. During unclamping, the diode is reverse biased and behaves as an open circuit. The resistance then introduces a time constant $\tau = R \cdot C_{NU}$ (or $\tau = R \cdot C_{NC}$) into the system and slows its average ramp rate relative to the input signal.

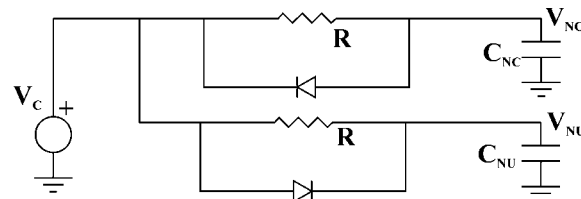


Fig 3: Delay Circuit

3. DYNAMIC MODEL

The dynamic model is composed of the lumped parameter model representing the piezoworm, the extension piezostack model, the clamp model, the delay circuit model and the friction model.

3.1 Lumped Parameter Model of the Piezoworm

A lumped parameter model was developed of the piezoworm from Fig. 1 and is shown in Fig. 4. This model is similar to that found in [3-5] except that part of the piezoworm is fixed and the moving member was added with its mass and external force. The equations of motion for the system depend on the friction state between the moving member and the clamps. There are four dynamic cases which are shown in Table 1. The right clamp section and the moving member with masses m_R and m_C , have displacements x_R and x_C and velocities v_R and v_C . Note that the left clamp mass, m_L , is fixed in this design. The right clamp section is

driven by the piezostack force, F_p , which is resisted by the return spring k_R and internal damping c_R . The clamps interact with the moving member through the friction forces F_{FL} and F_{FR} . The force F_d is external to the system and acts as a disturbance.

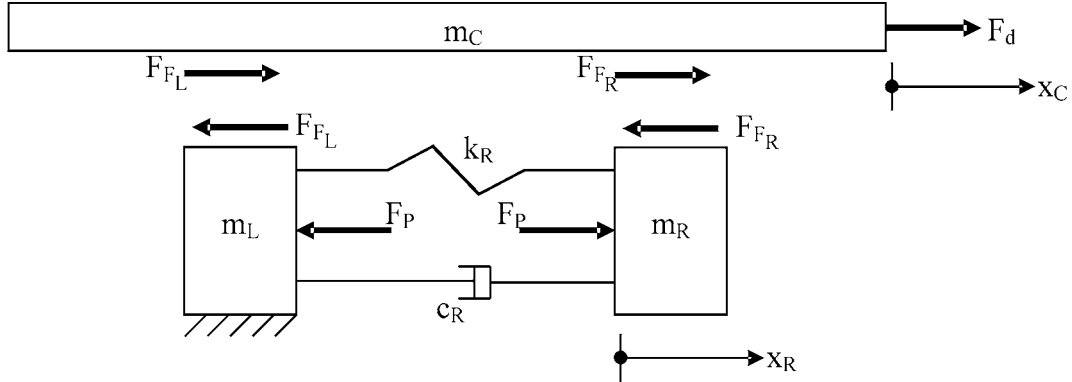


Fig. 4: Piezoworm Lumped Parameter Model

Table 1: Dynamic Model Cases

Dynamic Case	Friction State	Equation for m_R	Equation for m_C
1	both sliding	1	2
2	only m_L sliding	3	4
3	only m_R sliding	1	5
4	no sliding	4	5

$$m_R \ddot{x}_R = F_p - c_R \dot{x}_R - k_R x_R - F_{FR} \quad (1)$$

$$m_C \ddot{x}_C = F_{FR} + F_{FL} + F_d \quad (2)$$

$$(m_R + m_C) \ddot{x}_R = F_p - c_R \dot{x}_R - k_R x_R + F_{FL} + F_d \quad (3)$$

$$\ddot{x}_C = \ddot{x}_R \quad (4)$$

$$\ddot{x}_C = 0 \quad (5)$$

3.2 Extension Piezostack Model

The extension piezostack controls the position of the right mass, and indirectly, the moving member through the friction force (discussed in sub-Section 3.5). A linear model was adopted based on the IEEE piezoelectric linear model [11] and is shown in (6) where k_p is the piezostack stiffness, L_o is the piezostack free expansion at the maximum voltage V_{max} and V_{ext} is the applied voltage.

$$F_p = \frac{k_p L_o}{V_{max}} V_{ext} - k_p x_R \quad (6)$$

3.3 Clamp Model

The clamp voltages, V_{NU} and V_{NC} , the clamp characteristic slopes, m_{FVNU} and m_{FVNC} , and thresholds, V_{TNU} and V_{TNC} (see Fig. 2a and 2b) determine the maximum friction forces,

F_{FmaxNU} and F_{FmaxNC} , the clamps can provide. As previously mentioned, there exists a gap between the clamp surface and the moving member to allow complete disengagement given the tolerances of assembly and manufacture which gives rise to the threshold voltages. The clamp model is described by (7) and (8). In this design, the left clamp is NC and the right is NU so their maximum friction is renamed F_{FmaxL} and F_{FmaxR} and is used in the friction model.

$$F_{FmaxNU} = \begin{cases} 0 & \text{for } V_{NU} < V_{TNU} \\ m_{FVNU}(V_{NU} - V_{TNU}) & \text{for } V_{NU} \geq V_{TNU} \end{cases} \quad (7)$$

$$F_{FmaxNC} = \begin{cases} m_{FVNC}(V_{NC} - V_{TNC}) & \text{for } V_{NC} < V_{TNC} \\ 0 & \text{for } V_{NC} \geq V_{TNC} \end{cases} \quad (8)$$

3.4 Delay Circuit Model

The delay circuit model relates the clamp voltages to the common clamp voltage signal. For the circuit in Fig. 3, the transfer function in the Laplace domain is given by:

$$V_{NU,NC}(s) = \begin{cases} \frac{1}{sRC_{NUI,NC} + 1} V_C(s) & \text{delay active} \\ V_C(s) & \text{diode active} \end{cases} \quad (9)$$

3.4 Friction Model

Friction was incorporated using a stiction plus Coulomb friction model [12] with a constant coefficient of friction as shown in Fig. 4. If the sliding surfaces have a relative velocity, v_{rel} , greater than the threshold, v_o , then the friction force, F_f , is the maximum the clamp can provide (F_{FmaxL} or F_{FmaxR}). If they have a relative velocity less than the threshold, then the friction force is proportional to the applied load, $F_{applied}$, in order to maintain a relative velocity of zero up to the maximum friction of the clamp. This is summarized in (10) [12]. The small threshold velocity, v_o , is used in the simulation instead of zero to aid simulation algorithm convergence.

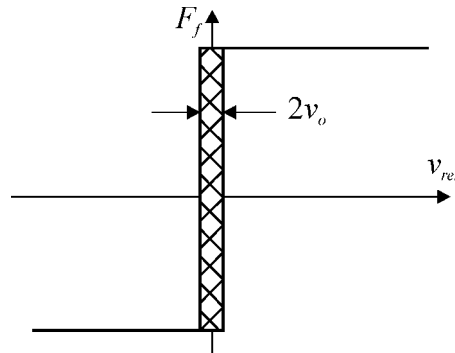


Fig. 4: Stiction + Coulomb Friction model

$$F_F = \begin{cases} F_{F_{\max}} \operatorname{sgn}(v_{rel}) & |v_{rel}| \geq v_o \\ F_{applied} \operatorname{sat}\left(\frac{F_{F_{\max}}}{F_{applied}}\right) & |v_{rel}| < v_o \end{cases} \quad (10)$$

The sign and saturation functions are given by:

$$\operatorname{sgn}(z) = \begin{cases} 1 & z > 0 \\ 0 & z = 0 \\ -1 & z < 0 \end{cases} \quad \operatorname{sat}(z) = \begin{cases} 1 & z > 0 \\ z & -1 \leq z \leq 1 \\ -1 & z < -1 \end{cases} \quad (11)$$

The two clamps and the moving member can have a possible seven cases for the friction F_{FL} and F_{FR} . When the relative velocity between the moving member and a clamp is less than the threshold, their velocities may be considered equal provided that the friction between them is below the maximum. The different cases are shown in Table 2. The cases are evaluated in sequence, particularly cases 4 to 7.

Table 2: Friction Model Cases

Case	Condition	F_{FR}	F_{FL}
1	$v_L \neq v_C$ & $v_R \neq v_C$	$\operatorname{sgn}(v_R - v_C) F_{F_{\max R}}$	$\operatorname{sgn}(-v_C) F_{F_{\max L}}$
2	$v_L \neq v_C$ & $v_R = v_C$	$[m_C(F_P - F_{iR}) - m_R(F_{FL} + F_d)] / (m_R + m_C)$	$\operatorname{sgn}(-v_C) F_{F_{\max L}}$
3	$v_L = v_C$ & $v_R \neq v_C$	$\operatorname{sgn}(v_R - v_C) F_{F_{\max R}}$	$-F_{FR} - F_d$
4	$v_C = v_R = 0$ both stuck	$F_P - F_{iR}$	$F_{iR} - F_P - F_d$
5	$v_C = v_R = 0$ m_R stuck	$[m_C(F_P - F_{iR}) - m_R(F_{FL} + F_d)] / (m_R + m_C)$	$\operatorname{sgn}(F_{FL\text{-case4}}) F_{F_{\max L}}$
6	$v_C = v_R = 0$ m_L stuck	$\operatorname{sgn}(F_{FR\text{-case4}}) F_{F_{\max R}}$	$-F_{FR} - F_d$
7	$v_C = v_R = 0$ none stuck	$\operatorname{sgn}(F_{FR\text{-case4}}) F_{F_{\max R}}$	$\operatorname{sgn}(F_{FL\text{-case4}}) F_{F_{\max L}}$

where: $F_{iR} = c_R v_R + k_R x_R$

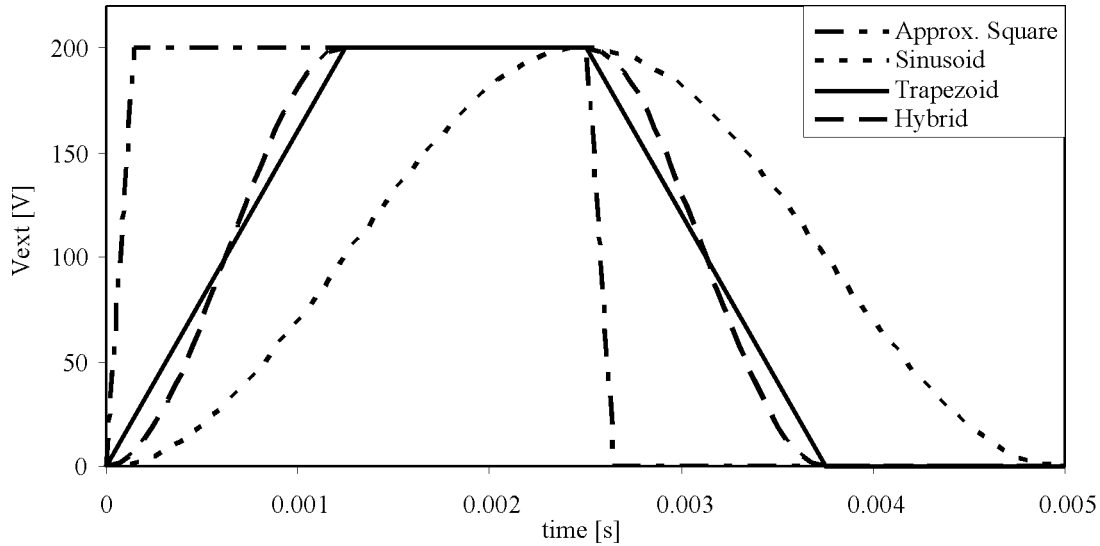
4. WAVEFORM ASSESSMENT

The model was constructed in Simulink [13] and used to assess the piezoworm performance for different waveform shapes and for delay circuit resistances. The inputs to the model are the common clamp voltage, V_C , the extender voltage, V_{ext} , and the disturbance force, F_d . The model parameters used in the simulation are given in Table 3.

Table 3: Model Parameters

Parameter	Value	Parameter	Value
m_R	0.2 kg	L_o	16 μm
k_R	0.667 N/ μm	k_P	121 N/ μm
c_R	146 N·s/m	V_{TNU}	20 V
m_C	0.016 kg	m_{FVNU}	0.2 N/V
V_{max}	200 V	V_{TNC}	180 V
v_o	1e-4 m/s	m_{FVNC}	-0.2 N/V
$C_{NU,NC}$	430 nF		

The four waveforms that were evaluated are: sinusoidal, trapezoidal, approximate square (trapezoid with steep ramps) and hybrid (trapezoidal with sinusoids for ramps) (see Fig. 5). A pure square wave cannot be achieved in practice because of the current limit of the power amplifier. A ramp rate for 0–200 V of 150 μs was used for the approximate square waveform. The ramp rate for the trapezoid and hybrid waveforms was 1.25 ms. The drive frequency was constant at 200 Hz since this will be used for future prototype testing.

**Fig 5: Waveforms used in simulation**

The performance was judged based on no-load speed, dynamic force capacity and relative no-load sliding wear rate. The dynamic force capacity was determined by increasing F_d until the piezoworm could not move in the intended direction. The sliding wear rate is proportional to the sliding length and friction force and was determined by (12)[14]. It is used as a relative measure of the wear that would be found in the piezoworm.

$$\text{wear rate} \propto \frac{\int |v_C F_{FL}| dt + \int |(v_R - v_C) F_{FR}| dt}{x_C} \quad (12)$$

The results of the simulation are given in Table 4. While the approximate square wave had much higher velocity than the waveforms, it came at a price of high wear and low force capacity. The reason is that the fast ramp rate accelerated the moving member to a point where its inertia overwhelmed the clamp friction and continued to slide along the clamp at the end of the cycle. The other three signals are closely matched in velocity and force capacity. However, the hybrid waveform, with its selective clamping and smooth ramps, had a very low relative wear rate.

Table 4: Waveform Performance Without the Delay Circuit

Waveform	Velocity [mm/s]	Force Capacity [N]	Wear Rate (N•m/m)
approx. square	7.59	5.8	84.02
sinusoid	3.14	31.9	3.58
trapezoid	3.19	31.6	1.62
hybrid	3.17	32.3	0.07

The hybrid waveform was tested with several values for R in the delay circuit to observe the effect on performance. Results in Table 5 show that the circuit increased the force capacity of the piezoworm while only marginally affecting the velocity and wear rate. A resistance of 300 Ω optimizes the performance for this actuator's parameters.

Table 5: Delay Circuit Performance With Hybrid Waveform

Resistance [Ω]	Velocity [mm/s]	Force Capacity [N]	Wear Rate (N•m/m)
1	3.17	32.3	0.07
300	3.17	35.7	0.05
600	3.17	35.9	0.09
800	3.17	35.6	0.30

5. CONCLUSIONS

The dynamic model of the step-and-repeat piezoworm actuator showed that the best waveform of those studied is the hybrid waveform. This waveform is a trapezoidal wave with sinusoids in the ramp portions. While a square waveform will give high velocity, the wear and force capacity are undesirable. The delay circuit increased the force capacity of the inchworm without detrimental effect on the velocity and wear rate. A resistance of 300 Ω is optimum for the parameters in the current design.

ACKNOWLEDGEMENT

This work was supported by the Canadian Space Agency under the STDP Program.

REFERENCES

1. B. Zhang and Z. Zhu, "Developing a linear piezomotor with nanometer resolution and high stiffness," IEEE/ASME Trans. on Mechatronics, vol. 2, pp.22-29, 1997.
2. R. Ben Mrad, A. Abhari and J. Zu, "A control methodology for an inchworm piezomotor," J. of Mechanical Systems and Signal Processing, vol. 17, 2003, pp. 457-71.
3. J. Frank, G. Koopmann, W. Chen and G. Lesieutre, "Design and Performance of a High Force Piezoelectric Inchworm Motor," Proc. SPIE - The International Society for Optical Engineering, vol. 3668, Newport Beach, March 1999, pp. 717-723.
4. D. Newton, E. Garcia and G. Horner, "A Linear piezoelectric Motor," Smart Materials and Structures, vol. 7, no. 3, 1998, pp. 295-304.
5. S. Ling, H. Du, T. Jiang, "Analytical and Experimental Study on a Piezoelectric Linear Motor," Smart Materials and Structures, vol. 7, no. 3, 1998, pp. 382-388.
6. J. Kim; J-D. Kim and S-B Choi, "A Hybrid Inchworm Linear Motor," Mechatronics, vol. 12, 2002, pp. 525-42.
7. S. Dong, L. Li, Z. Gui T. Zhou and X. Zhang, A New Type of Linear Piezoelectric Stepper Motor," IEEE Trans. on Components, Packaging and Manufacturing Technology Part A, vol. 18, no. 2, 1995, pp. 257-260.
8. S. Salisbury, D. F. Waechter, R. Ben Mrad, S. Eswar Prasad, R. G. Blacow, and B. Yan, "Design considerations for complementary inchworm actuators," IEEE Trans. on Mechatronics, in press.
9. A. Dogan, K. Uchino, and R. E. Newnham, "Composite piezoelectric transducer with truncated conical endcaps cymbal," IEEE Trans. on Ultrasonics, Ferroelectrics, and Frequency Control, vol. 44, no. 3, May 1997, pp. 597-605.
10. P. E. Tenzer and R. Ben Mrad, "On amplification in inchworm precision positioners," Mechatronics, vol. 14, issue 5, June 2004, pp. 515-531.
11. IEEE Standard on Piezoelectricity, ANSI/IEEE Standard 176-1987.
12. D. Karnoop, "Computer simulation of stick-slip friction in mechanical dynamic systems," ASME J. of Dynamic Systems, Measurements and Control, vol. 107, no. 1, 1985, pp. 100-103.
13. Simulink, Mathworks, Version 6.5 Release 13.
14. B. Bhushan, Ed., Modern Tribology Handbook, New York, CRC Press, 2001.